Tetrahedron 65 (2009) 7730–7740

Contents lists available at ScienceDirect

Tetrahedron

journal homepage: www.elsevier.com/locate/tet

Syntheses, structural and antimicrobial studies of a new *N*-allylamide of monensin A and its complexes with monovalent metal cations

Daniel Łowicki [a], Adam Huczyński [a], Joanna Stefańska [b], Bogumil Brzezinski [a,*]

[a] *Faculty of Chemistry, Adam Mickiewicz University, Grunwaldzka 6, 60-780 Poznan, Poland*
[b] *Medical University, Department of Pharmaceutical Microbiology, Oczki 3, 02-007 Warsaw, Poland*

ARTICLE INFO

Article history:
Received 25 March 2009
Received in revised form 28 May 2009
Accepted 19 June 2009
Available online 24 June 2009

Keywords:
Ionophores
Antibacterial activity
Complexes
Monovalent cations
Hydrogen bonds

ABSTRACT

A new *N*-allylamide of monensin A (M-AM2) was synthesized and its capacity to form complexes with Li^+, Na^+ and K^+ cations was studied by ESI MS, ^1H and ^{13}C NMR, FTIR spectroscopy and PM5 semi-empirical methods. ESI mass spectrometry indicates that M-AM2 forms complexes with Li^+, Na^+ and K^+ of exclusively 1:1 stoichiometry which are stable up to cv=70 V, and the formation of 1:1 complexes between M-AM2 and Na^+ cations is strongly favoured. Above cv=90 V we observe fragmentation of the respective complexes involving several dehydration steps. The spectroscopic studies show that the structures of the M-AM2 and its complexes with Li^+, Na^+ and K^+ cations are stabilized by intramolecular hydrogen bonds in which the OH groups are always involved. The data also demonstrate that the C=O amide group is engaged in the complexation process of each cation. However with the K^+ cation we also found a structure in which this C=O amide group does not participate in the complexation to a significant extent. The *in vitro* biological tests of M-AM2 amide show its good activity towards some strains of Gram-positive bacteria (Giz 13–19 mm; MIC 25–100 μg/ml).

1. Introduction

Monensin A, besides monensin B and other metabolites produced by various strains of *Streptomyces cinnamonensis*, is a well known natural polyether antibiotic.[1–3] Monensin acid exists in a pseudo-cyclic structure due to the formation of hydrogen bonds between the carboxylic group on the one side of the molecule and two hydroxyl groups on the opposite side.[4] The polyether skeleton of the pseudo-cyclic structure is able to form complexes with metal cations,[5–10] similar to some artificial analogues, such as crown ethers.[11–13] The lipophilic exterior of the monensin A molecule enables transport of the metal complexes across biological membranes.[14–16] Because of these properties, monensin A shows various biological activities such as the growth inhibition of Gram positive micro-organisms and control of chicken coccidiosis, for which it is applied commercially.[17,18] Despite these interesting and useful effects, the application of monensin A as a therapeutic or antimicrobial agent is limited because of a number of serious side-effects. A convenient way to obtain less toxic compounds based on monensin A is its conversion into esters or other derivatives, which show lower median lethal dose (LD_{50}) values than parent monensin while maintaining or even enhancing the biological activities.[19] Recently, we described the synthesis of some new esters and one amide of monensin A. We reported on their ability to form complexes with monovalent and divalent metal cations and their biological activities.[20–34] Antimicrobial studies of monensin A esters demonstrate that only three of them, including allyl ester, show antibacterial activity against human pathogenic bacteria.[31] The antimicrobial activity was shown to depend on the substituted group (allyl group) and therefore allylamine was also chosen as a substrate in the synthesis of a new *N*-allylamide of monensin A.

In this contribution we describe the synthesis and the spectroscopic as well as semiempirical characterization of a new *N*-allylamide of monensin A (M-AM2) and its complexes with metal cations in solution.

2. Results and discussion

The structures of monensin A (MONA) and the *N*-allylamide of monensin A (M-AM2) together with the atom numbering are shown

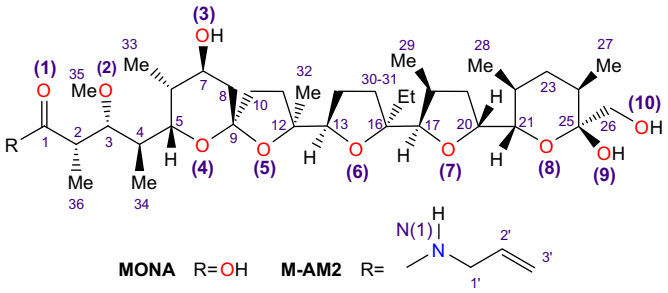

Scheme 1. The structures and atom numbering of MONA and M-AM2.

* Corresponding author.
E-mail address: bbrzez@main.amu.edu.pl (B. Brzezinski).

0040-4020/$ – see front matter © 2009 Elsevier Ltd. All rights reserved.
doi:10.1016/j.tet.2009.06.077

Table 1
The main peaks in the ESI mass spectra of the complexes of M-AM2 with cations at various cone voltages

Cation	Cone voltage [V]	Main peaks *m*/*z*
Li^+	10	717
	30	717
	50	717
	70	717
	90	717, 699, 681, 485, 467,445, 427, 220
	110	717, 699, 681, 485, 467,445, 427, 220
	130	717, 699, 681, 485, 467,445, 427, 220
Na^+	10	733
	30	733
	50	733
	70	733
	90	733, 715
	110	733, 715, 697, 507, 501, 489, 483, 479, 461, 443, 236
	130	733, 715, 697, 507, 501, 489, 483, 479, 461, 443, 236
K^+	10	749
	30	749
	50	749
	70	749
	90	749
	110	749, 731, 713
	130	749, 731, 713

in Scheme 1. M-AM2 amide was synthesized by condensing monensic acid with allylamine in the presence of 1,3-dicyclohexylcarbodiimide (DCC) with the addition of 1-hydroxybenzotriazole (HOBt) as a catalyst. This one-pot reaction led to M-AM2 with a good yield (67%). It is interesting to note that in the absence of the HOBt catalyst, under the same reaction conditions, no amide was formed.

2.1. Electrospray mass spectrometry (ESI) measurements

The main *m*/*z* signals in the ESI mass spectra of M-AM2 with the Li^+, Na^+ and K^+ cations used separately at various cone voltages are collected in Table 1 and one exemplary ESI mass spectrum of the 1:1 complex of M-AM2 with Li^+ cation measured at various cone voltages is shown in Figure 1. According to these data, M-AM2 forms exclusively complexes of 1:1 stoichiometry with metal cations and the complexes are very stable up to about cv=70 V. At cv=90 V, the fragmentation of the respective complexes is observed. The proposed fragmentation pathways starting from structure **A** are depicted in Scheme 2. The first step of the fragmentation is the loss of one water molecule as a result of loss of O(3)H or O(9)H hydroxyl groups yielding **B** or **H** cations, respectively. The regioselectivity of loss of the first water molecule, especially in formation of cation **B**, can be explained by strong engagement of the electron from O(3) atom in complexation of the

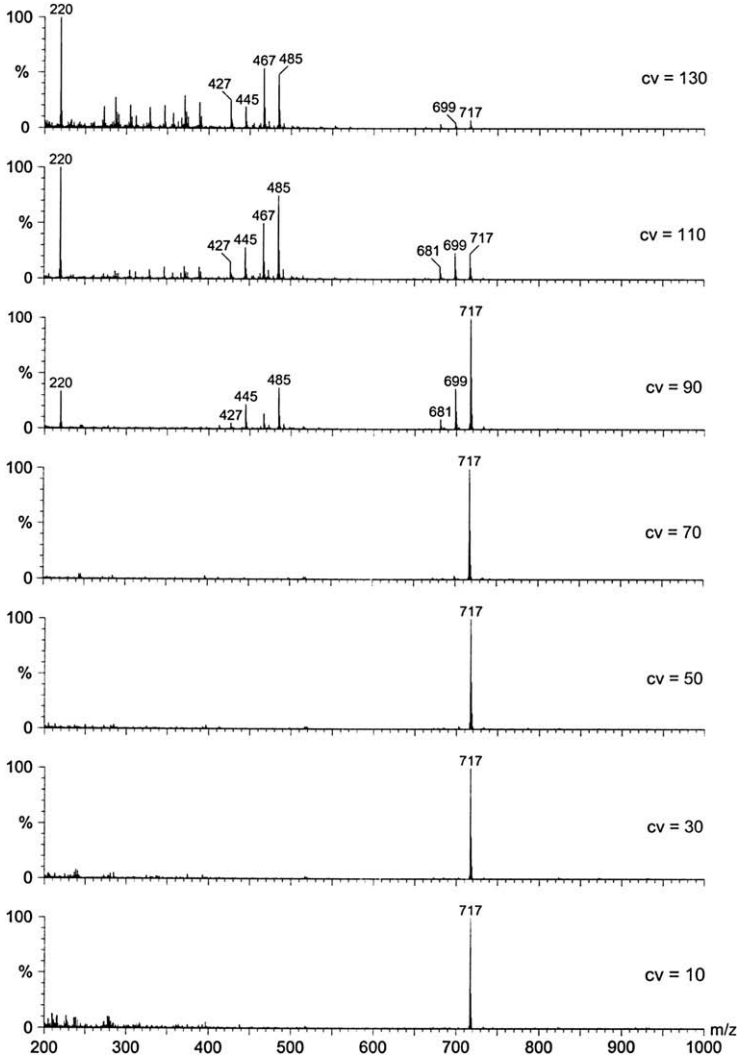

Figure 1. ESI mass spectra of 1:1 mixture of M-AM2 with Li^+ at various cone voltages (cv).

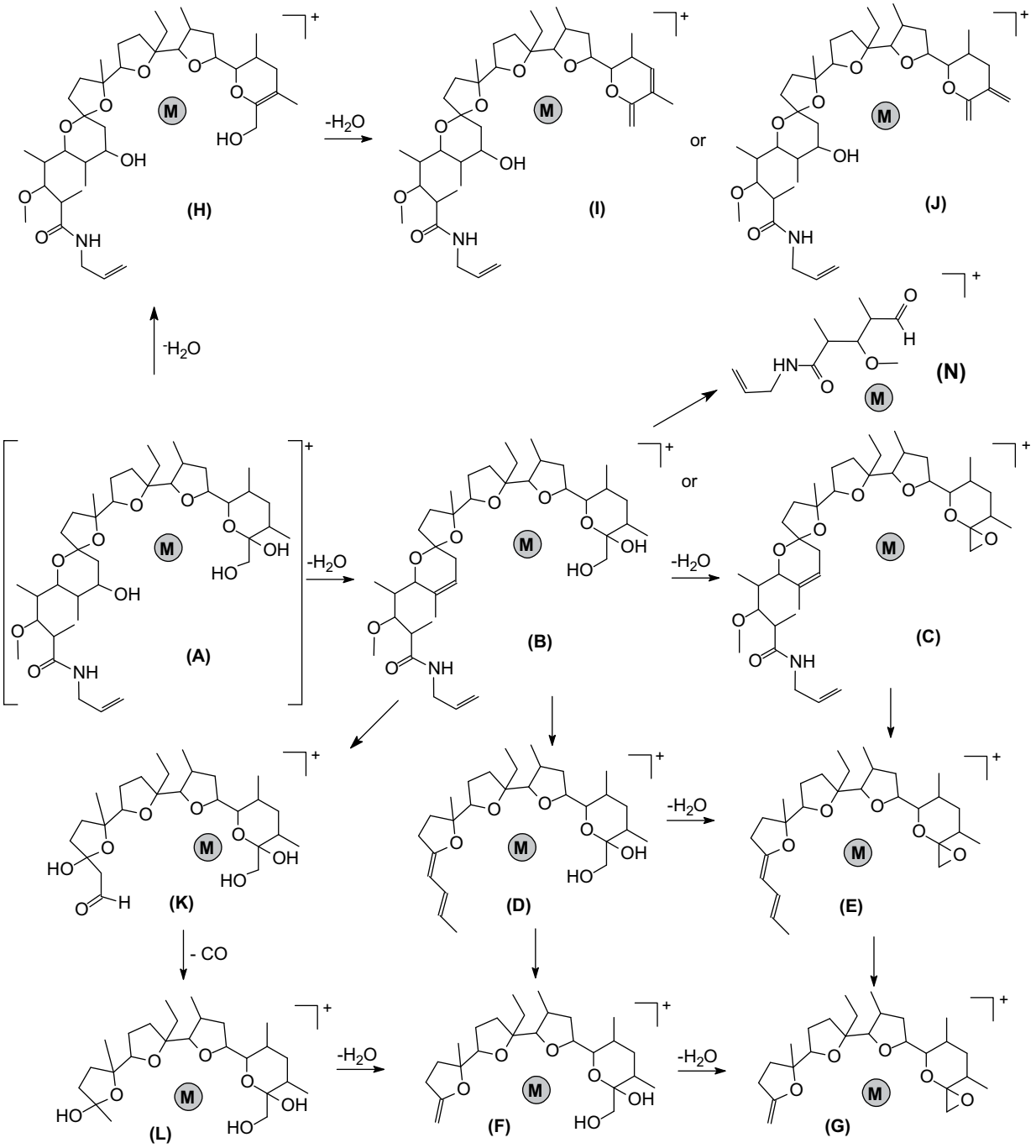

A		B, H		C, I, J		D		E	
$M=Li^+$	m/z=717	$M=Li^+$	m/z=699	$M=Li^+$	m/z=681	$M=Li^+$	m/z=485	$M=Li^+$	m/z=467
$M=Na^+$	m/z=733	$M=Na^+$	m/z=715	$M=Na^+$	m/z=697	$M=Na^+$	m/z=501	$M=Na^+$	m/z=483
$M=K^+$	m/z=749	$M=K^+$	m/z=731	$M=K^+$	m/z=713				

F		G		L		K		N	
$M=Li^+$	m/z=445	$M=Li^+$	m/z=427	$M=Na^+$	m/z=479	$M=Na^+$	m/z=507	$M=Li^+$	m/z=220
$M=Na^+$	m/z=461	$M=Na^+$	m/z=443					$M=Na^+$	m/z=236

Scheme 2. The proposed fragmentation pathways of M-AM2 complexes with monovalent cations.

metal cation. This is in accordance with the previously published data on the three-dimensional structure of monensin A,[35] and its derivatives in the solid and gas states,[8–10,41] as well as in the solution.[20–31] A similar regioselectivity of the dehydratation steps was also previously observed for monensin sodium salt and was lengthy discussed in the literature.[35–37]

Cation **H** yields cations **I** or **J** by loss of a second water molecule. Further fragmentation of cation **B**, of M-AM2 with Li^+ and Na^+

cations, is realized in two directions with the formation of other types of complexes (**C**, **D**, **E**, **F** and finally **G**). The epoxide structures of cations **C**, **E** and **G** have been previously postulated by Lopes et al.[35] Furthermore, cation **B** can undergo fragmentation to cation **N** due to complexation of Li^+ and Na^+ cations by the part of molecule with the amide group. Cation **C** is formed from cation **B** by loss of the second water molecule. The formation of **D** and **E** fragmentary complexes is achieved by abstraction of the part of the molecule with the amide moiety. The discussed fragmentation pathways correspond very well with those proposed for the salts of monensin described in Refs. 35–37. It has been demonstrated that the common fragmentation ions were produced via a Grob–Wharton type mechanism.[35]

Cations **F** and **G** can be formed from cations **D** and **E**, respectively, by abstraction of one C_3H_4 group. Additionally, cation **G** can be formed by loss of one water molecule from cation **F**. For the complex of M-AM2 with K^+ cation no abstraction of the part of the molecule which contains the amide group was detected.

For the M-AM2–Na^+ complex, an additional pathway (**A**→**B**→**K**→**L**) takes place. The cation **K** at *m*/*z* 507 is form via Grob–Wharthon fragmentation,[35] which after the abstraction of one CO molecule, forms cation **L**. Further, cation **L** undergoes fragmentations typical of other cations with abstraction of further water molecules yielding cations **F** and **G**, respectively.

Figure 2 presents the ESI spectrum of the 1:1:1:3 mixture of Li^+, Na^+, K^+ cations with M-AM2 measured at cv=30 V. In this figure only three characteristic signals at *m*/*z*=717, *m*/*z*=733 and *m*/*z*=749 assigned to the 1:1 complexes of M-AM2 with Li^+, Na^+ and K^+ cations are shown, respectively. The intensity of the M-AM2–Na^+ complex signal is the strongest, clearly indicating that M-AM2 preferentially forms complexes with Na^+ cations. The intensities of the signals of M-AM2–Li^+ and M-AM2–K^+ complexes are comparable, but significantly lower than that of M-AM2-Na^+ complex, demonstrating that M-AM2 shows much lower affinity to Li^+ and K^+ cations.

2.2. ^{1}H and ^{13}C NMR measurements

The ^{1}H and ^{13}C NMR data of M-AM2 and its 1:1 complexes with Li^+, Na^+ and K^+ cations all in CD_3CN are shown in Tables 2 and 3, respectively. Unfortunately, in contrast to the Li^+, Na^+ and K^+ complexes, the respective M-AM2 complexes with the $RbClO_4$ and $CsClO_4$ salts are almost insoluble in acetonitrile. The ^{1}H and ^{13}C NMR signals were assigned using one- and two-dimensional (COSY, HETCOR) spectra as well as by the addition of CD_3OD to the sample.

In the ^{1}H NMR spectra of M-AM2 and its 1:1 complexes with Li^+, Na^+ and K^+ cations (Table 2), the signals of the protons of all three OH groups are separate and their chemical shifts depend on the kind of the cation, as illustrated in Figure 3. In the spectrum of M-AM2 the OH proton signals observed at 4.00 ppm, 3.89 ppm and 2.86 ppm, are assigned to the O(3)H, O(9)H and O(10)H groups, respectively, whereas in the spectra of the complexes between M-AM2 and the Li^+, Na^+ and K^+ cations these signals are shifted in different directions depending on the cation. The most significantly shifted signal of all the OH groups is found in the spectrum of M-AM2–Na^+ complex at 6.40 ppm assigned to O(9)H proton. However, in the spectrum of M-AM2–Li^+ complex the most shifted signal is that of the O(3)H proton found at 6.10 ppm. Both these signals are involved in the strongest intramolecular hydrogen bonds in comparison with other hydroxyl groups. In contrast, in the spectra of the M-AM2 complexes with Na^+ and K^+ cations, the signals of the O(3)H protons are shifted towards lower ppm values indicating that the hydrogen bonds, in which the O(3)H protons are involved, are weaker. This demonstrates that depending on the kind of the cation, the respective hydroxyl groups form different intramolecular hydrogen bonds and therefore the complexes exhibit different structures.

A comparison of the ^{13}C NMR chemical shifts in the spectra of the complexes with those observed in the spectrum of M-AM2 (Table 3) suggests that the involvement of the oxygen atoms in the cations' coordination evokes some conformational changes. For instance the value of Δ at the C20 atom in the complex of M-AM2 with Li^+ cation is positive, for the complex of M-AM2 with Na^+ cation it is negative and for the M-AM2–K^+ complex it is almost unchanged. This result indicates that O(7) oxygen atom is involved in the coordination only in the complex of M-AM2 with Na^+ cation.

The ^{1}H and ^{13}C NMR chemical shifts of M-AM2 amide in CD_3CN and CD_2Cl_2 are compared in Table 4. In the ^{1}H NMR spectrum of M-AM2 in CD_2Cl_2, compared with that in CD_3CN, significant changes in the chemical shifts are detected for the O–H protons: the O(3)–H and O(9)–H protons become involved in slightly stronger hydrogen bonds and the O(10)–H proton is involved in a slightly weaker hydrogen bond. Also for the compound in CD_2Cl_2, the signal of the N–H proton shifts towards smaller ppm values relative to that in the spectrum taken in CD_3CN solvent. This indicates that the N–H proton is not involved in an intramolecular hydrogen-bond but only slightly stronger hydrogen-bonded to the CD_3CN molecules. This interpretation is consistent with the observations made on the basis of the FTIR spectra discussed below.

Comparison of the ^{13}C NMR chemical shifts of M-AM2 in both solvents indicates that the changes in the strength of hydrogen bonds within the structures cause also conformational changes and probably also charge distributions at some carbon atoms.

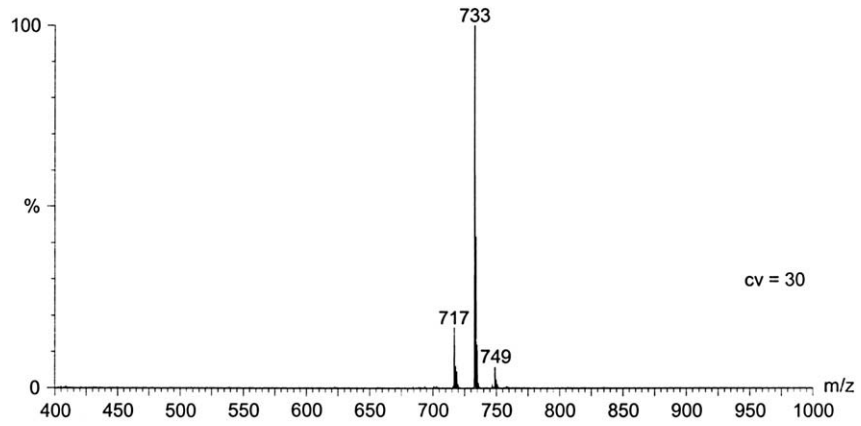

Figure 2. ESI mass spectrum of 1:1:1:3 mixture of cation perchlorates $LiClO_4$, $NaClO_4$ and $KClO_4$ with M-AM2 (cv=30 V).

Table 2
^{1}H NMR chemical shifts (ppm) of M-AM2 and its complexes in CD_3CN

No. Atom	Chemical shift (ppm)				Differences (Δ) between chemical shifts (ppm)		
	M-AM2	M-AM2–Li^+	M-AM2–Na^+	M-AM2–K^+	Δ1	Δ2	Δ3
1	—	—	—	—	—	—	—
2	2.43	2.51	2.64	2.51	0.08	0.21	0.08
3	3.35	3.40	3.38	3.33	0.05	0.03	−0.02
4	1.96	2.21	2.20	2.06	0.25	0.24	0.10
5	3.98	4.23	4.00	3.90	0.25	0.02	−0.08
6	1.78	1.64	1.60	1.62	−0.14	−0.18	−0.16
7	3.65	3.96	3.84	3.83	0.31	0.19	0.18
8A	1.60	1.98	1.64	1.58	0.38	0.04	−0.02
8B	1.99	2.06	2.02	2.01	0.07	0.03	0.02
9	—	—	—	—	—	—	—
10A	1.84	1.82	1.82	1.75	−0.02	−0.02	−0.09
10B	1.84	2.04	2.05	1.90	0.20	0.21	0.06
11A	1.71	1.85	1.86	1.92	0.14	0.15	0.21
11B	1.97	2.01	1.98	2.01	0.04	0.01	0.04
12	—	—	—	—	—	—	—
13	3.64	3.67	3.65	3.54	0.03	0.01	−0.10
14A	1.56	1.48	1.51	1.50	−0.08	−0.05	−0.06
14B	1.76	1.92	1.92	1.78	0.16	0.16	0.02
15A	1.57	1.51	1.49	1.47	−0.06	−0.08	−0.10
15B	2.10	2.20	2.30	2.20	0.10	0.20	0.10
16	—	—	—	—	—	—	—
17	3.86	4.25	3.90	3.95	0.39	0.04	0.09
18	2.25	2.38	2.33	2.33	0.13	0.08	0.08
19A	1.52	1.60	1.64	1.55	0.08	0.12	0.03
19B	2.15	2.23	2.18	2.17	0.08	0.03	0.02
20	4.20	4.42	4.40	4.38	0.22	0.20	0.18
21	3.57	3.90	3.82	3.74	0.33	0.25	0.17
22	1.32	1.40	1.45	1.36	0.08	0.13	0.04
23A	1.33	1.38	1.42	1.45	0.05	0.09	0.12
23B	1.43	1.41	1.58	1.73	−0.02	0.15	0.30
24	1.62	1.38	1.60	1.79	−0.24	−0.02	0.17
25	—	—	—	—	—	—	—
26A	3.36	3.43	3.50	3.39	0.07	0.14	0.03
26B	3.36	3.69	3.70	3.67	0.33	0.34	0.31
27	0.84	0.87	0.82	0.82	0.03	−0.02	−0.02
28	0.86	0.86	0.82	0.83	0.00	−0.04	−0.03
29	0.96	0.96	0.89	0.95	0.00	−0.07	−0.01
30A	1.54	1.50	1.51	1.50	−0.04	−0.03	−0.04
30B	1.54	1.71	1.74	1.69	0.17	0.20	0.15
31	0.92	0.94	0.92	0.90	0.02	0.00	−0.02
32	1.31	1.52	1.48	1.44	0.21	0.17	0.13
33	0.85	0.92	0.91	0.88	0.07	0.06	0.03
34	0.98	1.02	1.00	0.99	0.04	0.02	0.01
35	3.32	3.35	3.26	3.35	0.03	−0.06	0.03
36	1.12	1.20	1.20	1.19	0.08	0.08	0.07
1′	3.73	3.80	3.78	3.78	0.07	0.05	0.05
2′	5.90	5.85	5.82	5.85	−0.05	−0.08	−0.05
3′A	5.08	5.08	5.05	5.10	0.00	−0.03	0.02
3′B	5.18	5.16	5.12	5.20	−0.02	−0.06	0.02
N(1)H	6.68	7.00	6.86	6.96	0.32	0.18	0.28
O(3)H	4.00	6.10	3.89	3.88	2.10	−0.11	−0.12
O(9)H	3.89	4.24	6.40	2.51	0.35	2.51	−1.38
O(10)H	2.86	4.35	4.16	3.84	1.49	1.30	0.98

$\Delta1=\delta_{\text{M-AM2–Li}^+}-\delta_{\text{M-AM2}}$, $\Delta2=\delta_{\text{M-AM2–Na}^+}-\delta_{\text{M-AM2}}$, $\Delta3=\delta_{\text{M-AM2–K}^+}-\delta_{\text{M-AM2}}$.

Table 3
^{13}C NMR chemical shifts (ppm) of M-AM2 and its complexes in CD_3CN

No. Atom	Chemical shift (ppm)				Differences (Δ) between chemical shifts (ppm)		
	M-AM2	M-AM2–Li^+	M-AM2–Na^+	M-AM2–K^+	Δ1	Δ2	Δ3
1	175.48	178.87	179.03	177.20	3.39	3.55	1.72
2	42.96	42.92	42.50	43.58	−0.04	−0.46	0.62
3	82.67	80.10	80.19	82.33	−2.57	−2.48	−0.34
4	37.93	35.56	35.78	37.39	−2.37	−2.15	−0.54
5	68.37	69.74	69.50	68.09	1.37	1.13	−0.28
6	36.63	36.04	36.56	35.97	−0.59	−0.07	−0.66
7	71.94	70.16	70.54	70.76	−1.78	−1.40	−1.18
8	35.18	34.42	34.58	34.67	−0.76	−0.60	−0.51
9	108.37	108.23	108.51	108.26	−0.14	0.14	−0.11
10	39.91	39.68	39.77	39.88	−0.23	−0.14	−0.03
11	32.64	33.05	33.27	34.50	0.41	0.63	1.86
12	87.02	87.27	86.67	86.27	0.25	−0.35	−0.75
13	84.40	82.32	82.36	83.25	−2.08	−2.04	−1.15
14	28.66	27.25	27.18	27.94	−1.41	−1.48	−0.72
15	32.08	31.42	30.69	31.85	−0.66	−1.39	−0.23
16	88.05	87.61	86.85	86.89	−0.44	−1.20	−1.16
17	86.45	85.01	85.56	85.11	−1.44	−0.89	−1.34
18	35.87	34.13	35.05	35.34	−1.74	−0.82	−0.53
19	34.84	33.78	33.76	33.23	−1.06	−1.08	−1.61
20	78.16	78.86	76.97	78.13	0.70	−1.19	−0.03
21	77.33	74.62	75.96	75.61	−2.71	−1.37	−1.72
22	34.17	32.97	32.29	33.03	−1.20	−1.88	−1.14
23	37.72	36.43	36.03	36.80	−1.29	−1.69	−0.92
24	34.91	36.28	37.17	34.15	1.37	2.26	−0.76
25	98.00	99.16	98.69	98.92	1.16	0.69	0.92
26	67.45	66.98	66.99	66.94	−0.47	−0.46	−0.51
27	16.52	16.10	15.95	16.62	−0.42	−0.57	0.10
28	17.91	17.29	16.78	17.40	−0.62	−1.13	−0.51
29	16.21	15.56	14.27	15.67	−0.65	−1.94	−0.54
30	30.24	29.93	30.30	30.40	−0.31	0.06	0.16
31	8.34	8.24	8.14	8.46	−0.10	−0.20	0.12
32	26.16	28.42	28.35	28.08	2.26	2.19	1.92
33	11.26	10.35	10.56	10.68	−0.91	−0.70	−0.58
34	12.58	12.59	12.53	12.38	0.01	−0.05	−0.20
35	58.65	57.37	57.38	58.43	−1.28	−1.27	−0.22
36	14.71	13.58	13.92	14.77	−1.13	−0.79	0.06
1′	42.17	42.04	41.96	42.01	−0.13	−0.21	−0.16
2′	136.20	135.56	135.59	135.84	−0.64	−0.61	−0.36
3′	115.60	115.67	115.54	115.59	0.07	−0.06	−0.01

$\Delta1=\delta_{\text{M-AM2–Li}^+}-\delta_{\text{M-AM2}}$, $\Delta2=\delta_{\text{M-AM2–Na}^+}-\delta_{\text{M-AM2}}$, $\Delta3=\delta_{\text{M-AM2–K}^+}-\delta_{\text{M-AM2}}$.

2.3. FTIR studies

In Figure 4a the FTIR spectrum of water-free M-AM2 (solid line) is compared with the corresponding spectra of its 1:1 complexes with Li^+, Na^+ and K^+ cations, all recorded in acetonitrile solution. The regions of the ν(OH, NH) and ν(C═O) vibrations are additionally shown in Figure 4b and c, in an expanded scale, because according to the NMR data, the most significant changes should be observed in these spectral regions. Most characteristic, in the FTIR spectrum of water-free M-AM2 (Fig. 4b, solid, black line), are the bands assigned to the ν(OH) vibrations of the O(3)H, O(9)H and O(10)H groups at 3509 cm^{-1}, the ν(NH) vibrations of the N(1)H group at 3385 cm^{-1}, as well as the band assigned to the ν(C═O) vibrations at 1670 cm^{-1}. In the spectrum of the M-AM2–Li^+ complex (Fig. 4b, dashed blue line) the band at 3509 cm^{-1} vanishes and two bands arise at 3456 cm^{-1} and 3280 cm^{-1}. The first band is assigned to stretching vibrations of both O(10)H and O(9)H groups and the second one to the O(3)H group. This indicates that in the structure of M-AM2–Li^+ complex the hydrogen bonds of all O–H groups become slightly stronger when compared to those in the uncomplexed M-AM2 molecule. This interpretation is consistent with the ^{1}H NMR data (Table 2 and Fig. 3).

In the spectrum of M-AM2–Na^+ complex (Fig. 4b, dotted red line) a broad band with a maximum at ca. 3447 cm^{-1} is observed, demonstrating that the hydrogen bonds formed by the O(3)H and O(10)H groups become slightly stronger and that the hydrogen bond of the O(9)H group is the strongest one because the respective broad band shows a maximum at about 3261 cm^{-1}. Also in the spectrum of M-AM2–K^+ complex (Fig. 4b, dashed-dotted green line) only one band with a maximum at 3484 cm^{-1} is observed indicating that the hydrogen bonds, in which the hydroxyl groups are involved are almost unchanged as in the uncomplexed M-AM2. The position of the ν(NH) vibrations assigned to the N(1)H amide group is independent of the cation and is always observed at 3385 cm^{-1}. This observation is in agreement with the ^{1}H NMR data, because the N(1)H proton signal in the respective spectra of M-AM2 and in the spectra of its cation complexes is found about 7 ppm. The amide I and amide II bands in the FTIR spectrum of M-AM2 are observed at 1670 cm^{-1} and 1528 cm^{-1}, respectively

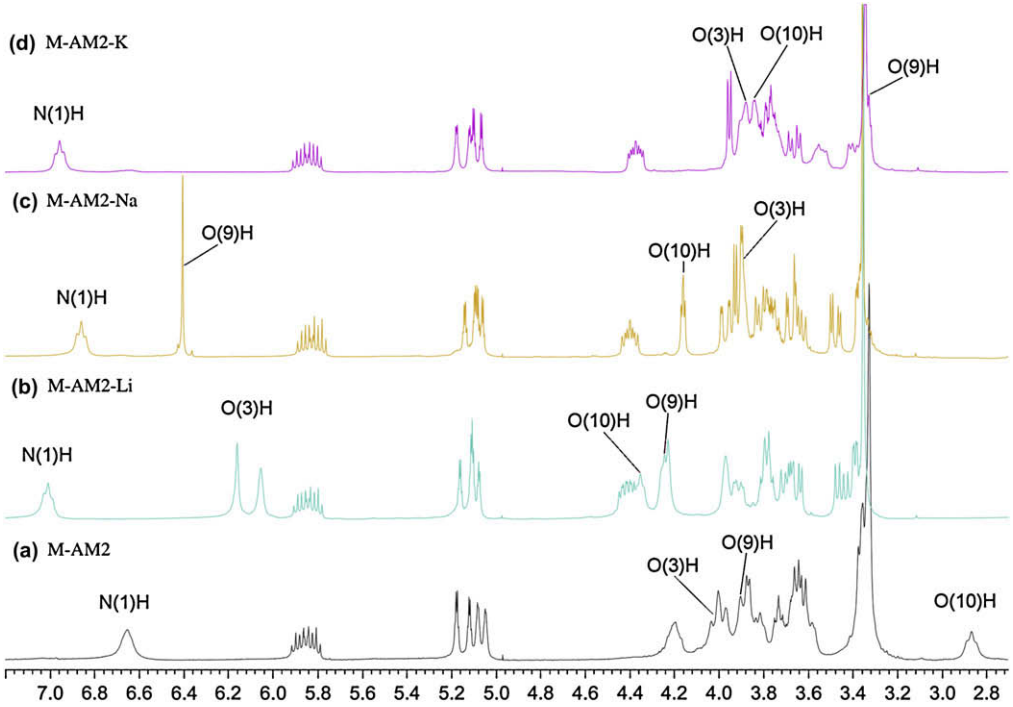

Figure 3. ^{1}H NMR in region of OH and NH proton signals of: (a) M-AM2, (b) M-AM2–Li^{+}, (c) M-AM2–Na^{+} and (d) M-AM2–K^{+} in CD_3CN.

(Fig. 4c). The positions of both bands change strongly with the formation of the complexes with metal cations. In the spectra of the M-AM2 complexes with Li^{+} and Na^{+} they are observed at 1637 cm^{-1} and 1542 cm^{-1}, respectively. In the spectrum of the M-AM2–K^{+} complex both amide I and amide II bands show a more complex character due to the existence of an equilibrium between two types of complexes in acetonitrile. In the first complex, the oxygen atom of the carbonyl group takes part in the complexation process while in the second one no contribution of this group is observed. The amide I bands observed in the spectra of M-AM2 complexes with Li^{+} and Na^{+} recorded under the same conditions show an intense shoulder around 1667 cm^{-1} indicating that the equilibrium described above still exists. However in contrast to the K^{+} complex, the Li^{+} and Na^{+} complexes predominantly exist in, a structure in which the carbonyl group is involved in the coordination process.

A hypothetical equilibrium between the complexed and the ligand-free form can be excluded by the NMR data, since none of the ^{1}H NMR spectra of the complexes (Fig. 3) exhibit the O(10)H signal at 2.86 ppm, typical of uncomplexed M-AM2. This unambiguously shows that the above described equilibrium only involves the M-AM2–cation complexes.

2.4. PM5 calculations

On the basis of the spectroscopic results, the heats of formation (HOF) of the structures of M-AM2 and its complexes with Li^{+}, Na^{+} and K^{+} cations were calculated (Table 5). Their values imply that the most stable complexes in the gas phase (under the experimental conditions similar to those of ESI measurements) are formed with $Na^{+}>>Li^{+}\approx K^{+}$ cations. This result is in good agreement with the ESI data discussed above. The ΔHOF values also show that the structures of M-AM2 with cations in which the carbonyl group is involved (structure B) are energetically more favourable than those in which the carbonyl group is not involved (structure A). The highest ΔHOF value is found for the M-AM2–Na^{+} complex of the structure B indicating that this structure is preferentially formed. Much lower is the ΔHOF value for the M-AM2–Na^{+} complex of the structure A showing that this structure also exists but is unfavourable. We made similar observations for the M-AM2–Li^{+} complex although the ΔHOF value is generally lower than that found for the respective M-AM2–Na^{+} complex. The lowest differences between the ΔHOF values of structures B and A are found for the M-AM2–K^{+} complex, −172.00 and −161.92 kcal/mol, respectively. These ΔHOF values indicate that both, structure A and B exist, whereas the structure B is slightly favoured. These results nicely corroborate the ESI data and the FTIR spectroscopic observations.

The interatomic distances between the oxygen atoms of M-AM2 and the cations together with the partial charges at these atoms are given in Table 6. Analysis of these values for structures B shows that some oxygen atoms such as O(1), O(3), O(5), O(6), O(8) and O(10) are always involved in the coordination of different metal cations, whereas only in the M-AM2–Na^{+} complex the O(7) atom does also play a role in this coordination process. For the complexes of A type structure in which the C(1)═O group is not involved in the complexation of the metal cation, the values of the calculated coordination distances are comparable with those in the B type structure. The results for the M-AM2–K^{+} complex given in Table 6 indicate that both types of complexes can be formed.

The calculated lengths and angles of the hydrogen bonds in which the OH groups are engaged are summarized in Table 7. The calculated structure of M-AM2 (Fig. 5) indicates that the O(1) oxygen atom of the C═O amide group is engaged in the bifurcated intramolecular hydrogen bonds with two O(9)H and O(10)H hydroxyl groups. With the formation of the respective B type complexes between M-AM2 and Li^{+}, Na^{+} and K^{+} cations (Figs. 6, 7 and 8a) these hydrogen bonds get broken because the O(1) oxygen atom is involved in the coordination process. For this reason the signal of the C(1) carbon atom in the ^{13}C NMR spectra of the complexes is shifted toward higher ppm values relative to its position in the spectrum of M-AM2 (Table 3). In the A structure of the M-AM2–K^{+} complex the C(1)═O carbonyl group is not involved in the coordination process and it is hydrogen bonded only to the O(10)H hydroxyl group (Fig. 8b). The hydrogen and the coordination bonds in the visualized structures of M-AM2 and its complexes with the

Table 4
^{1}H–^{13}C NMR chemical shifts (ppm) of M-AM2 in CD_2Cl_2 and CD_3CN

No. Atom	^{1}H NMR			^{13}C NMR		
	M-AM2 in CD_2Cl_2	M-AM2 in CD_3CN	Δ1	M-AM2 in CD_2Cl_2	M-AM2 in CD_3CN	Δ2
1	—	—	—	175.53	175.48	0.05
2	2.47	2.43	−0.04	42.69	42.96	0.27
3	3.37	3.35	0.02	82.48	82.67	0.19
4	2.00	1.96	−0.04	37.43	37.93	0.50
5	4.14	3.98	−0.16	67.65	68.37	0.72
6	1.74	1.78	0.04	36.99	36.63	0.36
7	3.75	3.65	−0.10	71.52	71.94	0.42
8A	1.63	1.60	−0.03	34.65	35.18	0.53
8B	1.98	1.99	0.01	—	—	—
9	—	—	—	107.94	108.37	0.43
10A	1.79	1.84	0.05	39.19	39.91	0.72
10B	1.95	1.84	−0.11	—	—	—
11A	1.81	1.71	−0.10	33.02	32.64	0.38
11B	1.87	1.97	0.10	—	—	—
12	—	—	—	85.86	87.02	1.16
13	3.58	3.64	0.06	83.51	84.40	0.89
14A	1.63	1.56	−0.07	28.00	28.66	0.66
14B	1.73	1.76	0.03	—	—	—
15A	1.52	1.57	0.05	31.27	32.08	0.81
15B	2.16	2.10	−0.06	—	—	—
16	—	—	—	86.89	88.05	1.16
17	3.84	3.86	0.02	86.22	86.45	0.23
18	2.24	2.25	0.01	35.31	35.87	0.56
19A	1.48	1.52	0.04	33.60	34.84	1.24
19B	2.12	2.15	0.03	—	—	—
20	4.26	4.20	−0.06	76.82	78.16	1.34
21	3.79	3.57	−0.22	75.64	77.33	1.69
22	1.37	1.32	−0.05	33.08	34.17	1.09
23A	1.40	1.33	−0.07	37.06	37.72	0.66
23B	1.40	1.43	0.03	—	—	—
24	1.60	1.62	0.02	35.19	34.91	0.28
25	—	—	—	97.48	98.00	0.52
26A	3.45	3.36	−0.09	67.79	67.45	0.34
26B	3.45	3.36	−0.09	—	—	—
27	0.84	0.84	0.00	16.45	16.52	0.07
28	0.85	0.86	0.01	17.47	17.91	0.44
29	0.94	0.96	0.02	15.63	16.21	0.58
30A	1.53	1.54	0.01	30.47	30.24	0.23
30B	1.53	1.54	0.01	—	—	—
31	0.92	0.92	0.00	8.39	8.34	0.05
32	1.43	1.31	−0.12	26.59	26.16	0.43
33	0.89	0.85	−0.04	11.15	11.26	0.11
34	1.01	0.98	−0.03	12.92	12.58	0.34
35	3.39	3.32	−0.07	58.70	58.65	0.05
36	1.18	1.12	−0.06	14.16	14.71	0.55
1′	3.81	3.73	−0.08	41.87	42.17	0.30
2′	5.85	5.90	0.05	135.28	136.20	0.92
3′A	5.07	5.08	0.01	115.27	115.60	0.33
3′B	5.14	5.18	0.04	—	—	—
N(1)H	6.49	6.68	0.19	—	—	—
O(3)H	4.49	4.00	−0.49	—	—	—
O(9)H	4.61	3.89	−0.72	—	—	—
O(10)H	2.75	2.86	0.11	—	—	—

(^{1}H NMR) $\Delta 1 = \delta_{\text{M-AM2(CD3CN)}} - \delta_{\text{M-AM2(CD2Cl2)}}$; ($^{13}C$ NMR) $\Delta 2 = \delta_{\text{M-AM2(CD3CN)}} - \delta_{\text{M-AM2(CD2Cl2)}}$.

Li^+, Na^+ and K^+ cations (Figs. 5–8) are marked by dots. A comparison of all the calculated structures indicates that only for the M-AM2 complex with Na^+ cation is the M-AM2 molecule able to form a pseudo-crown ether structure. This type of structure provides the most efficient interactions and therefore M-AM2 has the highest affinity to Na^+.

2.5. Antimicrobial activity

Monensin A (MONA) and its amide (M-AM2) were tested *in vitro* for their antibacterial and antifungal activity. The micro-organisms used in this study were as follows: Gram-positive bacteria, Gram-negative rods as well as yeasts. Monensin A and M-AM2 were efficient against Gram-positive bacteria but no activity against Gram-negative bacteria was detected. The antimicrobial properties of both MONA and M-AM2 are expressed by the minimum inhibitory concentration (MIC) as well as by the growth inhibition zone (Giz) (Table 8). Monensin A and M-AM2 show comparable activities against the human pathogenic bacteria (Giz 13–19 mm; MIC 25–100 μg/ml). However, both compounds are inactive against strains of *Candida* (*Candida albicans* and *Candida parapsilosis.*). The cell walls of Gram-negative bacteria do not permit the penetration of hydrophobic molecules with high molecular weights and thus these micro-organisms are not susceptible to the action of monensin and its allyl amide.

3. Conclusions

A new *N*-allylamide of monensin A (M-AM2) is a very good complexation agent especially for Na^+ cations, although it forms

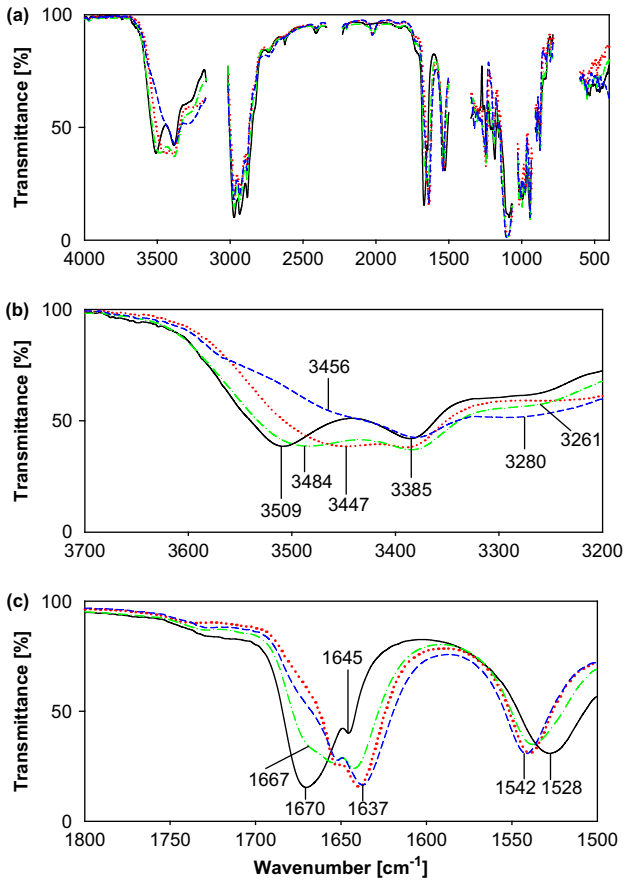

Figure 4. FTIR spectra of: (—) M-AM2, (---) M-AM2–Li^+, (···) M-AM2–Na^+, (-·-) M-AM2–K^+ in the ranges of: (a) 4000–400 cm^{-1}, (b) ν(OH)3800–3200 cm^{-1}, (c) ν(C=O) 1800–1500 cm^{-1} stretching vibrations recorded in CH_3CN.

Table 5
Heat of formation (kcal/mol) of M-AM2 and its complexes with the cations without (A) and with (B) the engagement of carbonyl group in coordination process calculated by PM5 method (WinMopac 2003)

Complex	HOF (kcal/mol)	ΔHOF (kcal/mol)
M-AM2	−565.00	
M-AM2+$Li^+_{uncomplexed}$ (A)	−442.26	−131.13
M-AM2+$Li^+_{complexed}$ (A)	573.39	
M-AM2+$Li^+_{uncomplexed}$ (B)	−442.26	−180.33
M-AM2+$Li^+_{complexed}$ (B)	−622.59	
M-AM2+$Na^+_{uncomplexed}$ (A)	−423.44	−144.17
M-AM2+$Na^+_{complexed}$ (A)	−576.61	
M-AM2+$Na^+_{uncomplexed}$ (B)	−423.44	−200.71
M-AM2+$Na^+_{complexed}$ (B)	−624.15	
M-AM2+$K^+_{uncomplexed}$ (A)	−448.56	−161.92
M-AM2+$K^+_{complexed}$ (A)	−610.48	
M-AM2+$K^+_{uncomplexed}$ (B)	−448.56	−172.00
M-AM2+$K^+_{complexed}$ (B)	−621.16	

$\Delta HOF = HOF_{M\text{-}AM2+M\ complexed} - HOF_{M\text{-}AM2+M\ uncomplexed}$, M—metal cation.
(A)—structure of M-AM2 complex in which the C1=O group is not involved in coordination of metal cation.
(B)—structure of M-AM2 complex in which the C1=O group is involved in coordination of metal cation.

Table 6
The interatomic distances (Å) and partial charges for O atoms of M-AM2 coordinating metal cations in complexes structures calculated by PM5 method (WinMopac 2003)

Complex with monovalent cation	Monovalent cation partial charge	Coordinating atom	Coordinating atom partial charge	Distance (Å) coordinating atom→cation
M-AM2–Li^+ (B type)	+0.439	O(1)	−0.371	2.17
		O(3)	−0.359	2.11
		O(5)	−0.428	2.11
		O(6)	−0.419	2.09
		O(8)	−0.411	2.19
		O(10)	−0.401	2.12
M-AM2–Na^+ (B type)	+0.308	O(1)	−0.435	2.37
		O(3)	−0.423	2.38
		O(5)	−0.383	2.37
		O(6)	−0.351	2.35
		O(7)	−0.370	2.32
		O(8)	−0.381	2.39
		O(10)	−0.394	2.39
M-AM2–K^+ (B type)	+0.481	O(1)	−0.403	2.86
		O(3)	−0.355	2.97
		O(5)	−0.258	2.85
		O(6)	−0.351	2.85
		O(8)	−0.244	2.91
		O(10)	−0.288	2.81
M-AM2–K^+ (A type)	+0.501	O(3)	−0.359	2.98
		O(5)	−0.279	2.94
		O(6)	−0.351	2.85
		O(8)	−0.233	2.87
		O(10)	−0.292	2.83

Table 7
The lengths (Å) and angles (°) of the hydrogen bond for M-AM2 and its complexes calculated by PM5 method (WinMopac 2003)

Compound	Type of structure*	Atoms engaged in hydrogen bonds	Length (Å)	Angle (°)
AM2		O(3)–H···O(8)	2.83	123.0
		O(9)–H···O(1)	2.72	125.7
		O(10)–H···O(1)	2.87	154.5
		N(1)–H···O(2)	2.93	128.6
M-AM2–Li^+	B	O(3)–H···O(8)	2.67	139.0
		O(9)–H···O(2)	2.75	138.3
		O(10)–H···O(2)	2.74	118.8
M-AM2–Na^+	B	O(3)–H···O(8)	2.82	117.1
		O(9)–H···O(3)	2.69	140.0
		O(10)–H···O(2)	2.92	135.3
M-AM2–K^+	B	O(3)–H···O(7)	2.82	124.1
		O(9)–H···O(2)	2.95	160.6
		O(10)–H···O(2)	2.74	116.1
M-AM2–K^+	A	O(3)–H···O(7)	2.89	128.1
		O(9)–H···O(2)	2.93	144.3
		O(10)–H···O(2)	2.75	116.2
		O(10)–H···O(1)	2.92	158.6

* A-structure of M-AM2 complex in which the C1=O group is not involved in coordination of metal cation. B-structure of M-AM2 complex in which the C1=O group is involved in coordination of metal cation.

also complexes with other monovalent cations. ESI mass spectrometry indicates that M-AM2 forms complexes with Li^+, Na^+ and K^+ of exclusively 1:1 stoichiometry which are stable up to cv=70 V. Above cv=90 V the fragmentation of the respective complexes involving some dehydration steps is observed. The structures of M-AM2 and its complexes with Li^+, Na^+ and K^+ cations are stabilized by relatively weak intramolecular hydrogen bonds in which the OH groups are always involved. In the structures of respective complexes the C=O amide groups are engaged in the complexation process. For the M-AM2–K^+ complex, an alternative structure in which this carbonyl group is not involved in the coordination process, was also observed. In contrast to the amide molecule in the structures of the ester complexes of monensin A the C=O ester group was generally not involved in the complexation process of the metal cations.[20–26] *In vitro* biological tests of M-AM2 amide show that this compound is active against some strains of Gram-positive bacteria (Giz 13–19 mm; MIC 25–100 μg/ml) and it is slightly more active than monensin A allyl ester.[23]

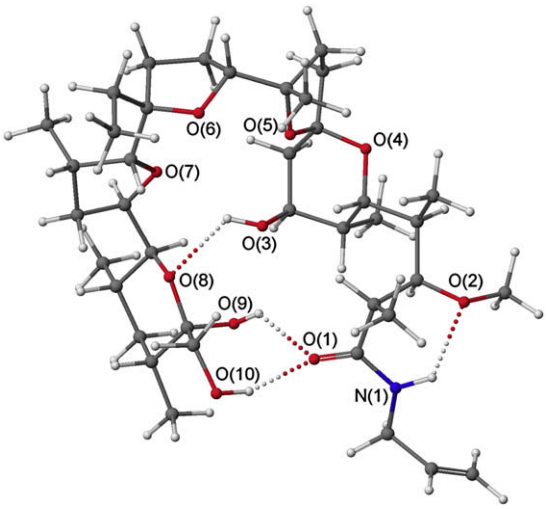

Figure 5. The structure of M-AM2 calculated by PM5 method (WinMopac2003).

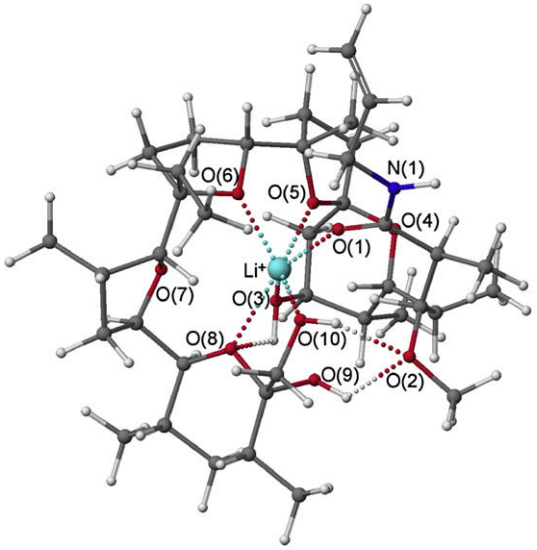

Figure 6. The structure of M-AM2–Li^+ complex calculated by PM5 method (WinMopac2003).

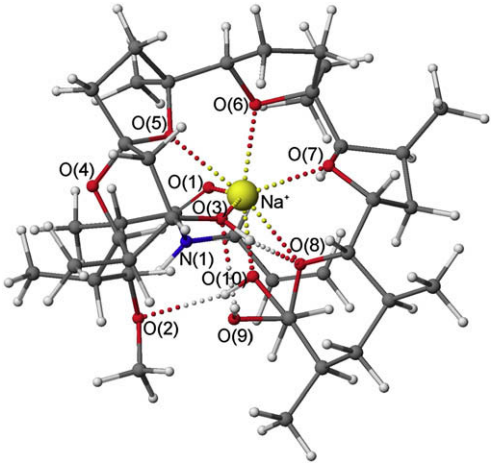

Figure 7. The structure of M-AM2-Na^+ complex calculated by PM5 method (WinMopac2003).

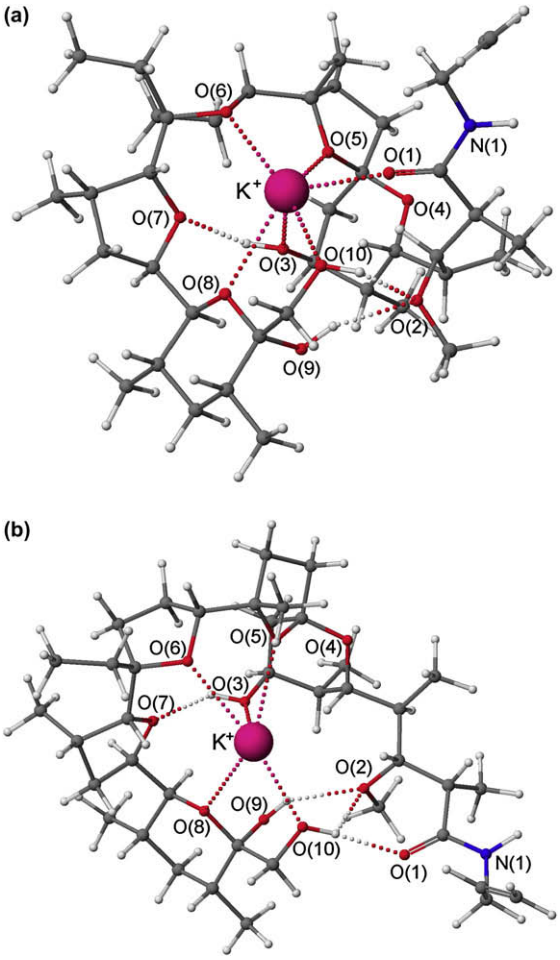

Figure 8. The structures of two types of M-AM2-K^+ complexes: (a) without the engagement of the C1═O carbonyl group in coordination of the cation—type A, (b) with the engagement of the C1═O carbonyl group in coordination of the cation—type B calculated by PM5 method (WinMopac 2003).

Table 8
Antimicrobial activity of MONA and M-AM2: diameter of the growth inhibition zone [Giz, mm] and minimal inhibitory concentration (MIC, μg/ml)

Tested strain	MONA		M-AM2	
	Giz (mm)	MIC (μg/ml)	Giz (mm)	MIC (μg/ml)
S. aureus NCTC 4163	22	2	17	50
S. aureus ATCC 25923	22	1	18	50
S. aureus ATCC 6538	20	2	17	50
S. aureus ATCC 29213	18	1	17	50
S. epidermidis ATCC 12228	15	2	19	100
B. subtilis ATCC 6633	22	1	19	50
B. cereus ATCC 11778	18	2	19	25
E. hirae ATCC 10541	—	12.5	—	>400
M. luteus ATCC 9341	12	4	16	50
M. luteus ATCC 10240	12	2	13	50

— denotes lack of the growth inhibition zone.

4. Experimental

4.1. General

Monensin A sodium salt was purchased from Sigma (90–95%). The perchlorates $LiClO_4$, $NaClO_4$ and $KClO_4$ were commercial products of Sigma and used without any further purification. Because the salts were hydrates, it was necessary to dehydrate them in several (6–10 times) evaporation steps from a 1:5 mixture of acetonitrile and absolute ethanol. The dehydration of the perchlorates was monitored by recording their FTIR spectra in acetonitrile.

CH_3CN, CD_3CN as well as CH_2Cl_2 and CD_2Cl_2 spectral-grade solvents were stored over 3 Å molecular sieves for several days. All manipulations with the substances were performed in a carefully dried and CO_2-free glove box.

4.2. Preparation of *N*-allylamide of monensin A (M-AM2) and its complexes with alkali metal cations

Monensin A sodium salt was dissolved in dichloromethane and stirred vigorously with a layer of aqueous sulfuric acid (pH=1.5). The organic layer containing MONA was washed with distilled water, and dichloromethane evaporated under reduced pressure to dryness to produce the acid.

A solution of MONA (1000 mg, 1.49 mmol), 1,3-dicyclohexylcarbodiimide (140 mg, 2.03 mmol), and allylamine (256 mg, 4.49 mmol) in dichloromethane and 1-hydroxybenzotriazole (330 mg, 2.16 mmol) dissolved in tetrahydrofuran were mixed together and stirred at a temperature between −4 °C to −5 °C for 24 h. After this time, the reaction mixture was stirred at room temperature for a further 24 h, diluted with H_2O and extracted with CH_2Cl_2. The extract was distilled under reduced pressure to dryness. The residue was suspended in hexane and filtered off to remove the 1,3-dicyclohexylurea by-product. The filtrate was evaporated under reduced pressure and purified by chromatography on silica gel (Fluka type 60) to give M-AM2 as a colourless solid (710 mg, 67% yield).

Elemental analysis: Calculated: C 65.98%, H 9.51%, N 1.97%. Found: C 66.03%, H 9.48%, N 1.91%.

4.3. Synthesis of M-AM2 complexes with monovalent cations

0.07 mol dm^{-3} solutions of the 1:1 complexes of M-AM2 with monovalent cations (Li^+, Na^+ and K^+) were obtained by adding equimolar amounts of $MClO_4$ salts (M=Li, Na, K) dissolved in acetonitrile to an acetonitrile solution of M-AM2. The solvent was evaporated under reduced pressure to dryness and the residue was dissolved in an appropriate volume of dry CH_3CN and CD_3CN to obtain the complex of the 0.07 mol dm^{-3} concentration.

4.4. ESI MS studies

The ESI (Electrospray Ionisation) mass spectra were recorded on a Waters/Micromass (Manchester, UK) ZQ mass spectrometer equipped with a Harvard Apparatus syringe pump. All samples were prepared in acetonitrile. The measurements were performed for solutions of M-AM2 (5×10^{-5} mol dm^{-3}) with: (a) each of the cations Li^+, Na^+ and K^+ (2.5×10^{-4} mol dm^{-3}) taken separately and (b) the cations Li^+, Na^+ and K^+ ($5\times10^{-5}/3$ mol dm^{-3}) taken together. The samples were infused into the ESI source using a Harvard pump at a flow rate of 20 μl min^{-1}. The ESI source potentials were: capillary 3 kV, lens 0.5 kV, extractor 4 V. The standard ESI mass spectra were recorded at the cone voltages: 10, 30, 50, 70, 90, 110 and 130 V. The source temperature was 120 °C and the desolvation temperature was 300 °C. Nitrogen was used as the nebulizing and desolvation gas at flow-rates of 100 and 300 dm^3 h^{-1}, respectively. Mass spectra were acquired in the positive ion detection mode with unit mass resolution at a step of 1 *m*/*z* unit. The mass range for ESI experiments was from *m*/*z*=200 to *m*/*z*=1000.

4.5. Spectroscopic measurements

The FTIR spectra of M-AM2 and its 1:1 complexes (0.07 mol dm^{-3}) with $LiClO_4$, $NaClO_4$, and $KClO_4$ were recorded in the mid infrared region in acetonitrile solutions using a Bruker IFS 113v spectrometer. The FTIR analysis of M-AM2 amide was also carried out in CH_2Cl_2 solution.

A cell with Si windows and wedge-shaped layers was used to avoid interferences (mean layer thickness 170 μm). The spectra were taken with an IFS 113v FT-IR spectrophotometer (Bruker, Karlsruhe) equipped with a DTGS detector; resolution 2 cm^{-1}, NSS=125. The Happ-Genzel apodization function was used. All manipulations with the compounds were performed in a carefully dried and CO_2-free glove box.

The NMR spectra of M-AM2 and its 1:1 complexes (0.07 mol dm^{-3}) with $LiClO_4$, $NaClO_4$ and $KClO_4$ were recorded in CD_3CN solutions using a Varian Gemini 300 MHz spectrometer. The NMR analysis of M-AM2 amide was also carried out in CD_2Cl_2 solution. All spectra were locked to the deuterium resonance of CD_3CN and CD_2Cl_2, respectively.

The ^1H NMR measurements in CD_3CN and CD_2Cl_2 were carried out at the operating frequency 300.075 MHz; flip angle, pw=45°; spectral width, sw=4500 Hz; acquisition time, at=2.0 s; relaxation delay, d_1=1.0 s; *T*=293.0 K and using TMS as the internal standard. No window function or zero filling was used. Digital resolution was 0.2 Hz per point. The error of chemical shift value was 0.01 ppm.

^{13}C NMR spectra were recorded at the operating frequency 75.454 MHz; pw=60°; sw=19,000 Hz; at=1.8 s; d_1=1.0 s; *T*=293.0 K and TMS as the internal standard. Line broadening parameters were 0.5 or 1 Hz. The error of chemical shift value was 0.01 ppm.

The ^1H and ^{13}C NMR signals were assigned independently for each species using one or two-dimensional (COSY, HETCOR) spectra.

4.6. PM5 calculations

PM5 semi-empirical calculations were performed using the WinMopac 2003 program. In all cases, full geometry optimisation of M-AM2 and its complexes was carried out without any symmetry constraints.[38–41]

4.7. Elemental analysis

The elemental analysis of M-AM2 was carried out on Vario ELIII (Elementar, Germany).

4.8. Microbiological analysis

Micro-organisms used in this study were as follows: Gram-positive cocci: *Staphylococcus aureus* NCTC 4163, *S. aureus* ATCC 25923, *S. aureus* ATCC 6538, *S. aureus* ATCC 29213, *Staphylococcus epidermidis* ATCC 12228, *Bacillus subtilis* ATCC 6633, *Bacillus cereus* ATCC 11778, *Enterococcus hirae* ATCC 10541, *Micrococcus luteus* ATCC 9341, *M. luteus* ATCC 10240; Gram-negative rods: *Escherichia coli* ATCC 10538, *E. coli* ATCC 25922, *E. coli* NCTC 8196, *Proteus vulgaris* NCTC 4635, *Pseudomonas aeruginosa* ATCC 15442, *P. aeruginosa* NCTC 6749, *P. aeruginosa* ATCC 27863, *Bordetella bronchiseptica* ATCC 4617 and yeasts: *C. albicans* ATCC 10231, *C. albicans* ATCC 90028, *C. parapsilosis* ATCC 22019. The micro-organisms used were obtained from the collection of the Department of Pharmaceutical Microbiology, Medical University of Warsaw, Poland.

Antimicrobial activity was examined by the disc-diffusion method under standard conditions using Mueller-Hinton II agar medium (Becton Dickinson) for bacteria and RPMI agar with 2% glucose (Sigma) according to CLSI (previously NCCLS) guidelines.[42]

Sterile filter paper discs (9 mm diameter, Whatman No 3 chromatography paper) were dripped with tested compound solutions (in MeOH or MeOH/DMSO 1:1) to load 400 μg of a given compound per disc. Dry discs were placed on the surface of appropriate agar medium. The results (diameter of the growth inhibition zone) were read after 18 h of incubation at 35 °C. Compounds which showed activity in disc-diffusion tests were examined by the agar dilution

method to determine their MIC—Minimal Inhibitory Concentration (CLSI).[43] Concentrations of the agents tested in solid medium ranged from 3.125 to 400 μg/ml. The final inoculum of all studied organisms was 10^4 CFU ml^{-1} (colony forming units per ml), except the final inoculum for *E. hirae* ATCC 10541, which was 10^5 CFU ml^{-1}. Minimal inhibitory concentrations were read after 18 h of incubation at 35 °C.

References and notes

1. Haney, M. E., Jr.; Hoehn, M. M. *Antimicrob. Agents Chemother.* **1967**, *7*, 349–352.
2. Westley, J. W.; Evans, R. H.; Sello, L. H.; Troupe, N.; Liu, C.; Miller, P. A. *J. Antibiot.* **1981**, *34*, 1248–1252.
3. Pospisil, S.; Sedmera, P.; Havlicek, V. *J. Antibiot.* **1996**, *49*, 935–937.
4. Lutz, W. K.; Winkler, F. K.; Dunitz, J. D. *Helv. Chim. Acta* **1971**, *54*, 1103–1108.
5. Martinek, T.; Riddell, F. G.; Wilson, C.; Weller, C. T. *J. Chem. Soc., Perkin Trans. 2* **2000**, 35–41.
6. Duax, W. L.; Smith, G. D.; Strong, P. D. *J. Am. Chem. Soc.* **1980**, *102*, 6725–6729.
7. Ward, D. L.; Wei, K. T.; Hoogerheide, J. C.; Popov, A. I. *Acta Crystallogr., Sect. B* **1978**, *34*, 110–115.
8. Huczyński, A.; Ratajczak-Sitarz, M.; Katrusiak, A.; Brzezinski, B. *J. Mol. Struct.* **2007**, *832*, 84–89.
9. Huczyński, A.; Ratajczak-Sitarz, M.; Katrusiak, A.; Brzezinski, B. *J. Mol. Struct.* **2007**, *871*, 92–97.
10. Huczyński, A.; Ratajczak-Sitarz, M.; Katrusiak, A.; Brzezinski, B. *J. Mol. Struct.* **2008**, *888*, 224–229.
11. Pedersen, C. J. *J. Am. Chem. Soc.* **1967**, *89*, 7017–7036.
12. Pedersen, C. J. *Angew. Chem., Int. Ed. Engl.* **1988**, *27*, 1021–1027.
13. Gokel, G. W. *Encyclopedia of Supramolecular Chemistry: Crown Ethers*; Marcel Dekker: Boca Raton, FL, USA, 2004; pp 326–333.
14. Mollenhauer, H. H.; Morre, D. J.; Rowe, L. D. *Biochim. Biophys. Acta* **1990**, *1031*, 225–246.
15. Nakazato, K.; Hatano, Y. *Biochim. Biophys. Acta* **1991**, *1064*, 103–110.
16. Riddell, F. G. *Chirality* **2002**, *14*, 121–125.
17. Stephan, B.; Rommel, M.; Daugschies, A.; Haberkorn, A. *Vet. Parasitol.* **1997**, *69*, 19–29.
18. Butaye, P.; Devriese, L. A.; Haesebrouck, F. *Clin. Microbiol. Rev.* **2003**, *16*, 175–188.
19. Westley, J. W.; Liu, C.; Evans, R. H.; Sello, L. H.; Troupe, N.; Hermannn, T. *J. Antibiot.* **1983**, *36*, 1195–1200.
20. Huczyński, A.; Przybylski, P.; Brzezinski, B.; Bartl, F. *Biopolymers* **2006**, *81*, 282–294.
21. Huczyński, A.; Przybylski, P.; Brzezinski, B.; Bartl, F. *Biopolymers* **2006**, *82*, 491–503.
22. Huczyński, A.; Michalak, D.; Przybylski, P.; Brzezinski, B.; Bartl, F. *J. Mol. Struct.* **2006**, *797*, 99–110.
23. Huczyński, A.; Michalak, D.; Przybylski, P.; Brzezinski, B.; Bartl, F. *J. Mol. Struct.* **2007**, *828*, 130–141.
24. Huczyński, A.; Łowicki, D.; Brzezinski, B.; Bartl, F. *J. Mol. Struct.* **2008**, *874*, 89–100.
25. Huczyński, A.; Przybylski, P.; Brzezinski, B. *Tetrahedron* **2007**, *63*, 8831–8839.
26. Huczyński, A.; Łowicki, D.; Brzezinski, B.; Bartl, F. *J. Mol. Struct.* **2008**, *879*, 14–24.
27. Huczyński, A.; Przybylski, P.; Brzezinski, B. *J. Mol. Struct.* **2006**, *788*, 176–183.
28. Huczyński, A.; Przybylski, P.; Schroeder, G.; Brzezinski, B. *J. Mol. Struct.* **2007**, *29*, 111–119.
29. Huczyński, A.; Brzezinski, B.; Bartl, F. *J. Mol. Struct.* **2008**, *886*, 9–16.
30. Huczyński, A.; Przybylski, P.; Brzezinski, B.; Bartl, F. *J. Phys. Chem. B* **2006**, *110*, 15615–15623.
31. Huczyński, A.; Stefańska, J.; Przybylski, P.; Brzezinski, B.; Bartl, F. *Bioorg. Med. Chem. Lett.* **2008**, *18*, 2585–2589.
32. Huczyński, A.; Domańska, A.; Paluch, I.; Stefańska, J.; Brzezinski, B.; Bartl, F. *Tetrahedron Lett.* **2008**, *49*, 5572–5575.
33. Huczyński, A.; Domańska, A.; Łowicki, D.; Brzezinski, B.; Bartl, F. *J. Mol. Struct.* **2009**, *920*, 414–423.
34. Łowicki, D.; Huczyński, A.; Ratajczak-Sitarz, M.; Katrusiak, A.; Stefańska, J.; Brzezinski, B.; Bartl, F. *J. Mol. Struct.* **2009**, *923*, 53–59.
35. Lopes, N. P.; Stark, C. B. W.; Gates, P. J.; Staunton, J. *Analyst* **2002**, *127*, 503–506.
36. Kiehl, D. E.; Julian, R. K.; Kennington, A. S. *Rapid Commun. Mass Spectrom.* **1998**, *12*, 903–910.
37. Lopes, N. P.; Stark, C. B. W.; Hong, H.; Gates, P. J.; Staunton, J. *Rapid Commun. Mass Spectrom.* **2002**, *16*, 414–420.
38. Stewart, J. J. P. *J. Comput. Chem.* **1989**, *10*, 209–220.
39. Stewart, J. J. P. *J. Comput. Chem.* **1991**, *12*, 320–341.
40. *CAChe 5.04 UserGuide*; Fujitsu: Beaverton, Oregon, 2003.
41. Przybylski, P.; Huczyński, A.; Brzezinski, B. *J. Mol. Struct.* **2007**, *826*, 156–164.
42. Clinical and Laboratory Standards Institute. *Performance Standards for Antimicrobial Disc Susceptibility Tests; Approved Standard M2-A9*; Clinical and Laboratory Standards Institute: Wayne, PA, USA, 2006.
43. Clinical and Laboratory Standards Institute. *Methods for Dilution Antimicrobial Susceptibility Tests for Bacteria That Grow Aerobically; Approved Standard M7-A7*; Clinical and Laboratory Standards Institute: Wayne, PA, USA, 2006.